

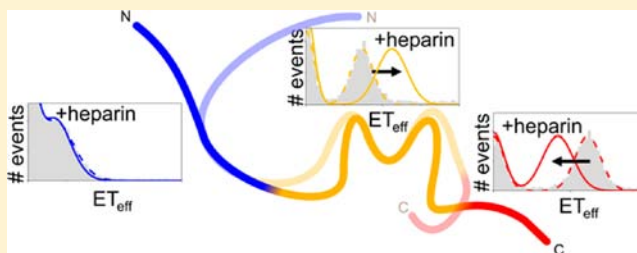
# Identification of an Aggregation-Prone Structure of Tau<sup>†</sup>

Shana Elbaum-Garfinkle and Elizabeth Rhoades\*

Department of Molecular Biophysics and Biochemistry, Yale University, 266 Whitney Avenue, New Haven, Connecticut 06520-8114, United States

**S** Supporting Information

**ABSTRACT:** The aggregation and deposition of normally soluble proteins is the hallmark of several devastating neurodegenerative disorders. For proteins such as tau in Alzheimer's disease and  $\alpha$ -synuclein in Parkinson's disease, aggregation involves a transition from an intrinsically disordered monomer to a highly structured fiber. While understanding the role of these proteins in neurodegeneration requires elucidation of the structural basis of self-association, the conformational heterogeneity of disordered proteins makes their structural characterization inherently challenging. Here we use single molecule Förster resonance energy transfer to measure the conformational ensemble of tau in the absence and presence of heparin to identify critical conformational changes relevant to the initiation of aggregation. We find that different domains of tau display distinct conformational properties that are strongly correlated with their degree of disorder and that may relate to their roles in aggregation. Moreover, we observe that heparin binding induces a distinct two-state structural transition in tau characterized by a loss of long-range contacts and a concomitant compaction of the microtubule binding domain. Our results describe a conformational intermediate of tau that precedes the formation of aggregates and could serve as a target for tau-focused therapeutics.



## INTRODUCTION

The tauopathies are a group of neurodegenerative disorders, including Alzheimer's disease (AD), the frontotemporal dementias, and chronic traumatic encephalopathy, characterized by the presence of proteinaceous aggregates called paired helical filaments (PHFs) and neurofibrillary tangles (NFTs). Tau is the primary component of PHFs and NFTs, and although the precise relationship between aggregate formation and disease pathology remains to be determined, the identification of point mutations in tau that result in hereditary tauopathies suggests a direct connection between tau misfunction and neurodegeneration.<sup>1–5</sup> Under physiological conditions, tau lacks stable secondary and tertiary structure,<sup>6,7</sup> while in PHFs and NFTs it adopts a highly ordered  $\beta$ -sheet rich structure.<sup>8</sup> Tau shares these features with other disordered proteins whose aggregation is implicated in disease, such as  $\alpha$ -synuclein in Parkinson's disease, islet amyloid polypeptide in type II diabetes, and  $A\beta$ , also implicated in AD (reviewed in ref 9).

The native function of tau is to stabilize microtubules (MTs) in the axons of the central nervous system, where it plays a major role in the establishment of normal neuronal morphology.<sup>6,10</sup> Binding of tau to MTs is mediated through its microtubule binding region (MTBR) and enhanced by the flanking proline-rich region and C-terminus<sup>11,12</sup> (Figure 1). The function of the N-terminal projection domain, which projects away from the MT surface, is not well-understood, although a number of putative binding partners, including actin

and the neuronal plasma membrane, have been suggested (reviewed in refs 2, 13) (Figure 1).

The MTBR forms the core of the PHFs<sup>14</sup> and fragments of tau consisting of the isolated MTBR exhibit accelerated aggregation as compared to the full-length protein.<sup>15</sup> In vitro, tau aggregation is induced by polyanionic compounds,<sup>16–20</sup> which lead to aggregates with the same general morphological characteristics as PHFs extracted from the AD brain.<sup>16,18–24</sup> One of the most commonly used molecular inducers is heparin, a highly negatively charged glycosaminoglycan, and recent efforts in therapeutics aimed at tau have focused on screening for compounds that inhibit heparin-induced filament formation.<sup>25,26</sup> It is now widely believed that it is the process of aggregation rather than the resulting fibrillar species that is responsible for the toxicity associated with the various tauopathies,<sup>27–30</sup> and it has been suggested that conformational changes that stabilize an assembly competent state are responsible for the initiation of tau aggregation.<sup>18</sup>

A molecular description of the aggregation pathway, including a detailed understanding of the conformational changes relevant to the initiation of aggregation, is thus crucial for developing a model of tau toxicity. These conformational changes, however, are inherently challenging to characterize. Monomer tau is disordered and highly dynamic in solution, and the changes in its conformational ensemble that precede aggregation do not necessarily involve populating well-defined

Received: May 31, 2012

Published: September 21, 2012

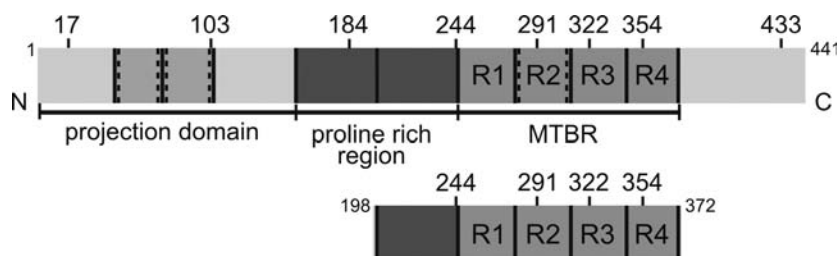


**Figure 1.** Tau schematic. The longest full-length tau isoform (top) and the K16 fragment (bottom) are pictured. Regions of interest indicated are the projection domain, the proline-rich region, and the MTBR (including the four repeats R1–R4). The residues mutated for labeling with fluorescent probes are shown above the schematic. Alternative splicing of two N-terminal exons and one exon in the MTBR give rise to six different tau isoforms (exon boundaries denoted with dashed lines).

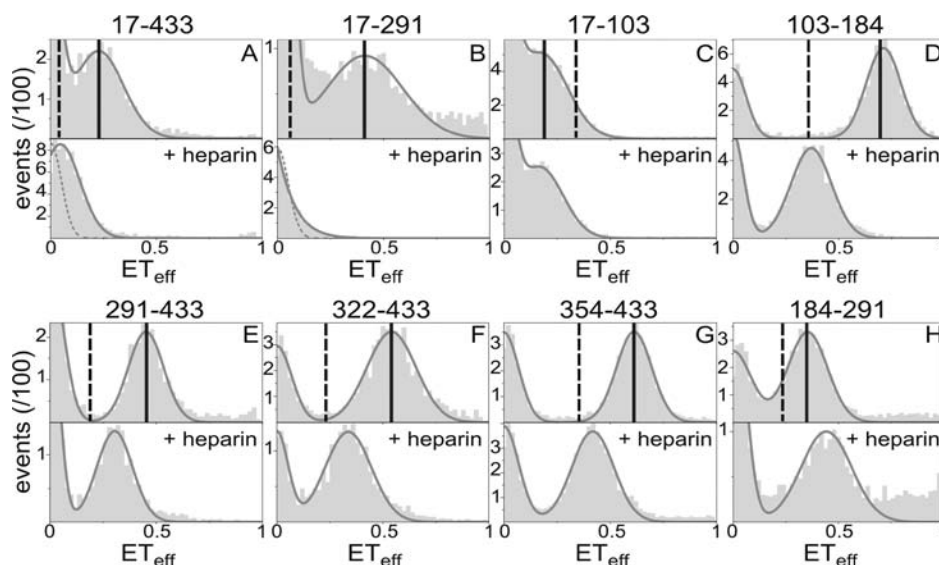


**Figure 2.** Single-molecule FRET histograms of eight full-length tau constructs. Representative  $ET_{\text{eff}}$  histograms are shown for constructs 17–433 (A), 17–291 (B), 17–103 (C), 103–184 (D), 291–433 (E), 322–433 (F), 354–433 (G), and 184–291 (H) in the absence (top panels) and in the presence of 10  $\mu\text{M}$  heparin (bottom panels). The mean measured  $ET_{\text{eff}}$  (solid line) and the theoretical  $ET_{\text{eff}}$   $\langle E \rangle$ , calculated for a model RC (dashed line) of each construct are indicated on the plots (see the text, SI, and Table 1). In the bottom panels of parts A and B the dotted gray line denotes the fit to a standard “zero-peak” to illustrate that the additional width in these distributions are due to a very low  $ET_{\text{eff}}$  signal.

secondary and tertiary structures. Moreover, solution conditions that favor aggregation-prone structures are also biased toward rapid aggregation such that, despite precautions, ensemble techniques may sample a heterogeneous mixture of oligomeric and monomer species rather than pure monomer. By contrast, the very low protein concentrations used in single molecule experiments strongly disfavor aggregation. Additionally, single-molecule Förster resonance energy transfer (FRET) is particularly well-suited to characterizing monomer ensembles because it can report on relative conformational changes in the absence of canonical structure.

In the current study, we use single-molecule FRET to identify conformational changes in tau that potentiate it for aggregation. In order to determine both global and local features, multiple overlapping regions of tau were individually measured in the absence and presence of heparin, which induces rapid aggregation of tau *in vitro*.<sup>31–33</sup> We find that different domains of tau exhibit distinct physicochemical and conformational properties that relate to their relative degree of disorder. Our results suggest that the release of long-range interactions and a concomitant compaction of the MTBR and proline-rich domain are the critical early conformational changes necessary for tau aggregation.

## EXPERIMENTAL SECTION

**Preparation and Labeling of Proteins.** Site-specific labeling was achieved by introducing cysteines at desired locations to enable attachment of maleimide reactive dyes Alexa Fluor 488 and 594. All full-length protein constructs included a cleavable His-tag to facilitate purification, while truncated constructs were purified as described previously.<sup>20</sup> See the Supporting Information (SI) for details.

**Single-Molecule FRET and FCS Measurements.** Single-molecule FRET and fluorescence correlation spectroscopy (FCS) measurements were made as described previously on a lab-built instrument based on an inverted Olympus IX-71 microscope (Olympus, Tokyo, Japan).<sup>20,34</sup> See SI for details.

## RESULTS

We generated 12 constructs of the longest tau isoform (Figure 1) by introducing cysteine mutations in pairs at specific sites throughout the protein sequence (see Experimental Section and SI). All constructs were labeled with the donor–acceptor fluorophore pair Alexa Fluor 488 and Alexa Fluor 594 (see Experimental Section and SI). Labeling positions were chosen to span specific domains and regions of interest within the tau sequence (Figure 1). Measurements were made of  $\sim 30$  pM protein, and the FRET efficiencies ( $ET_{\text{eff}}$ ) of individual, freely diffusing fluorescent molecules were calculated as  $ET_{\text{eff}} = I_A/(I_D$

Table 1.  $ET_{\text{eff}}$  of Tau in the Absence and Presence of Heparin<sup>a</sup>

C1	C2	no. of residues	$ET_{\text{eff}}$	$\langle E \rangle$	$\Delta ET_{\text{eff}}^b$	+ heparin	
						$ET_{\text{eff}}$	$\Delta ET_{\text{eff}}^c$
17	433	417	$0.22 \pm 0.02$	0.04	↑	<0.1	↓
17	291	275	$0.42 \pm 0.03$	0.08	↑	<0.1	↓
17	103	87	$0.17 \pm 0.01$	0.30	↓	$0.17 \pm 0.01$	—
103	184	82	$0.70 \pm 0.01$	0.32	↑	$0.35 \pm 0.02$	↓
103	291	189	$0.33 \pm 0.02$	0.13	↑	$0.14 \pm 0.04$	↓
291	433	143	$0.42 \pm 0.02$	0.18	↑	$0.30 \pm 0.02$	↓
322	433	112	$0.51 \pm 0.02$	0.24	↑	$0.35 \pm 0.02$	↓
354	433	80	$0.62 \pm 0.01$	0.33	↑	$0.39 \pm 0.02$	↓
291	322	32	$0.81 \pm 0.01$	0.64	↑	$0.81 \pm 0.01$	—
291	354	64	$0.61 \pm 0.01$	0.40	↑	$0.68 \pm 0.01$	↑
244	354	111	$0.37 \pm 0.01$	0.24	↑	$0.52 \pm 0.03$	↑
184	291	108	$0.36 \pm 0.01$	0.24	↑	$0.47 \pm 0.04$	↑

<sup>a</sup>The peak  $ET_{\text{eff}}$  measured for tau in the absence and presence of heparin and the mean  $ET_{\text{eff}}$   $\langle E \rangle$ , calculated for a theoretical RC model of the same number residues (as described in the text) are listed. C1 and C2 denote the positions of the fluorophores. <sup>b</sup> $\Delta ET_{\text{eff}}$  compares the peak  $ET_{\text{eff}}$  of tau in solution with the  $\langle E \rangle$  predicted for a random coil. <sup>c</sup> $\Delta ET_{\text{eff}}$  compares the peak  $ET_{\text{eff}}$  of tau with and without heparin bound. Errors denote the standard deviation from the mean of at least three independent experiments.

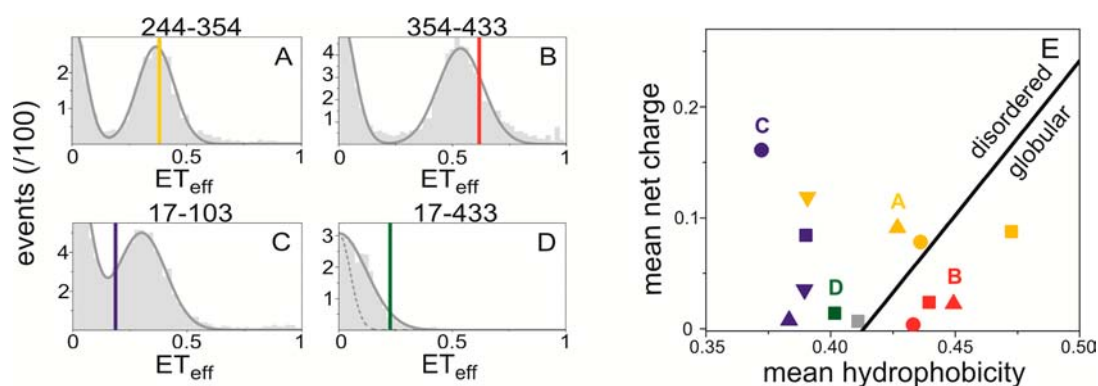


**Figure 3.** Charge screening by NaCl.  $ET_{\text{eff}}$  histograms in 500 mM NaCl are pictured for full-length constructs 244–354 (A), 354–433 (B), 17–103 (C), and 17–433 (D), with colored vertical lines indicating the peak position for each construct at 50 mM NaCl. (E) Mean net charge as a function of mean hydrophobicity for all constructs; the MTBR and proline-rich region constructs are in yellow, the C-terminal constructs are in red, the N-terminal constructs are in blue, the end-to-end construct 17–433 is in green, and the full-length protein is in gray.

+  $I_A$ ), where  $I_A$  and  $I_D$  are the intensities of the acceptor and donor fluorophores, respectively (see Experimental Section and SI). The  $ET_{\text{eff}}$  values were plotted as histograms and fit with a sum of Gaussian distributions to determine the peak  $ET_{\text{eff}}$  positions, as illustrated in Figure 2. The average number of events for each histogram is  $\sim 1000$ .

In order to compare the measured peak  $ET_{\text{eff}}$  for each construct to the theoretical mean  $ET_{\text{eff}}$   $\langle E \rangle$ , predicted from a random coil (RC) model for the same number of residues, we first calculated a radius of gyration,  $R_g$ , for each protein construct, assuming that it behaved as an RC, which was then used to calculate  $\langle E \rangle$  (SI). The measured peak  $ET_{\text{eff}}$  of each construct and the calculated  $\langle E \rangle$  for an ideal RC of the same length are listed in Table 1. The model of tau derived from the measurements is shown in Figure 5.

**Tau is Globally Compact with Long-Range Contacts.**  $ET_{\text{eff}}$  histograms of eight full-length tau constructs (Figure 2A–H) each have a single peak, characteristic of intrinsically disordered proteins<sup>34–38</sup> as well as of the chemically denatured states of globular proteins.<sup>38,39</sup> The overall dimensions of tau deviate significantly from those of a RC in a “good” solvent, with the termini considerably closer to each other than predicted from this model. The peak  $ET_{\text{eff}}$  of the longest construct (417 residues), which spans almost the entire protein

(residues 17–433; Figure 2A), is  $0.22 \pm 0.02$ . This construct would result in an  $ET_{\text{eff}}$  unresolved from the zero peak if tau behaved as an ideal RC (expected  $\langle E \rangle = 0.04$ ). The compact structure of tau suggested by the close contact between the N- and C-termini as seen with FRET is supported by FCS, which measures a diffusion time corresponding to a hydrodynamic radius,  $R_h$ , of 46 Å (SI).

Both termini are also in relatively close proximity to the MTBR. Specifically, the N-terminus is closer to R2 (residues 17–291, peak  $ET_{\text{eff}} = 0.42 \pm 0.03$ ; Figure 2B) than it is to the middle of the projection domain (residues 17–103, peak  $ET_{\text{eff}} = 0.17 \pm 0.01$ ; Figure 2C), despite being significantly further away in linear sequence (275 residues compared to 87 residues, respectively), indicating that the N-terminus folds toward the MTBR (Figure 5). Likewise, measurements of the MTBR and the C-terminus show that each of the repeat domains (R2, residues 291–433, Figure 2E; R3, residues 322–433, Figure 2F; and R4, residues 354–433, Figure 2G) are significantly closer to the C-terminus than expected for an ideal RC (Figure 5).

**Domains Have Distinct Conformational Characteristics.** Although tau is globally compact, the compaction is not uniformly distributed throughout the protein chain. In fact, our measurements show that the different domains of tau have distinct conformational properties: (a) the MTBR with the

adjacent proline-rich region is closest to a theoretical RC, with probes of this region showing only a minor deviation from the ideal model (Figure 2H and SI, Figure S1A,B); (b) the C-terminus is more compact than the model RC (Figure 2E–G); and (c) the first half of the N-terminal projection domain shows significant expansion relative to a RC (Figure 2C), while the second half of this domain shows a compensating compaction (Figure 2D). Recent NMR studies<sup>40,41</sup> support the presence of transient long-range interactions accompanied by distinct structural features within various domains of tau.

To further probe the region-specific differences noted above, we selected representative constructs and measured them in 500 mM NaCl (Figure 3A–D). Each construct responded in a distinctive manner: (a) no significant change was observed for the MTBR domain (Figure 3A); (b) the C-terminus construct shifted to lower  $ET_{\text{eff}}$  values, indicating expansion of this region (Figure 3B); (c) the first half of the N-terminal domain construct shifted to higher  $ET_{\text{eff}}$  values as a result of compaction (Figure 3C); and (d) there was no measurable energy transfer between the N- and C-termini, indicating a loss of long-range contacts and suggestive of an overall opening up of the protein (Figure 3D). This overall expansion is confirmed by FCS measurements in 500 mM NaCl, which show a change in diffusion time consistent with an increase in  $R_h$  of ~8%. These findings strongly support the idea that the relatively compact conformation of tau in solution can be attributed in part to the electrostatic attraction of the negatively charged termini to the positively charged MTBR and proline-rich regions.

**The Termini Modulate the MTBR.** The conformational ensemble of the MTBR region is altered by the presence of the flanking domains. Two MTBR constructs, one spanning the greater part of the MTBR (residues 244–354) and one probing the R2-R3 domain (residues 291–322), were measured in full-length tau and in isolation in the K16 fragment (Figure 1; SI, Figure S1). Both constructs show that the MTBR is more compact in isolation than it is in the full-length protein, as seen by higher peak  $ET_{\text{eff}}$  values in the histograms of K16 relative to full-length tau. Fragments of tau containing the MTBR, such as K16, demonstrate marked enhanced propensity for aggregation as compared to the full-length protein, and the presence of the termini has been suggested to inhibit specific interactions within the MTBR.<sup>42</sup>

**Heparin Binding Releases Long-Range Interactions and Compacts the MTBR.** Binding of heparin to tau results in marked conformational changes throughout the protein. The effects of heparin were determined by titrating it into a fixed concentration of tau (~30 pM) (SI). A transition between heparin-free and heparin-bound states was observed both for a MTBR-spanning construct as well as for a projection-domain construct (Figure 4). Initially only the free protein peak is observed, but with increasing heparin concentrations, the bound peak appears and grows while the free peak becomes less prominent and then disappears (Figure 4). The presence of two interchanging peaks is generally observed in single-molecule FRET measurements of equilibrium unfolding of two-state proteins<sup>43,44</sup> and is in marked contrast to the continuous expansion or compaction that has been reported for disordered proteins or denatured globular proteins in the presence of increasing salt or denaturant.<sup>37–39,45</sup> This suggests that the binding of heparin to tau results in the population of a distinct conformational state, as opposed to the continuous transition expected to result from simple charge screening. This

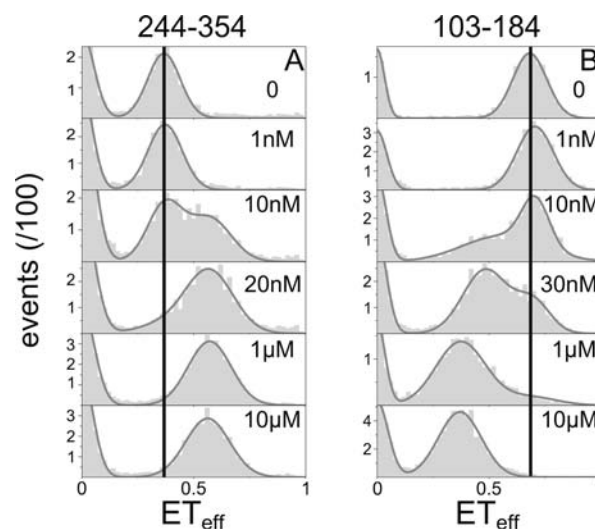


**Figure 4.** Heparin binding to tau. Titration of heparin into tau results in the appearance of a distinct peak upon binding of heparin. Notably, heparin binding causes compaction in one construct (A, 244–354) and expansion of the other (B, 103–184). The concentration of heparin is noted on each panel. For details on extracted binding curves see SI text and Figure S2.

continuous transition is observed in the “bound” peak of the projection domain construct (Figure 4B) which shifts from peak  $ET_{\text{eff}} \approx 0.49$  at 30 nM heparin to peak  $ET_{\text{eff}} \approx 0.37$  at 1  $\mu\text{M}$  heparin, possibly as a result of additional low-affinity interactions with heparin. From these titrations, we determined that tau has at least one very high affinity,  $K_D \approx 20$  nM, binding site for heparin (details in the SI), significantly tighter than what has previously been reported.<sup>46,47</sup> This is likely due to the low protein concentrations (~30 pM) used in our assays, which allow us to measure high-affinity (nM)  $K_D$  values much more accurately than the orders of magnitude higher tau concentrations (40–200  $\mu\text{M}$ ) used previously<sup>46,47</sup> (see SI for more details).

The remaining constructs were measured in the presence of 10  $\mu\text{M}$  heparin, a concentration where the heparin binding sites are expected to be close to saturated (Figure 4 and SI, text and Figure S2). Heparin binding leads to a shift to lower peak  $ET_{\text{eff}}$  values indicative of more expanded conformations for most of the constructs measured (Figure 2A,B,D–G), with an overall increase in  $R_h$  seen by FCS (SI). Notably, long-range contacts between the two termini and each terminus and the MTBR are reduced. This supports the idea that one of the consequences of heparin binding is to increase the solvent exposure of the aggregation-initiating components of the MTBR,<sup>48</sup> enhancing the probability for intermolecular contacts between these regions. It follows that long-range interactions between the termini in the heparin-free monomer may serve to shield these components and play an important role in abrogating protein aggregation.

Exceptions to the overall expansion noted above are seen in (a) compaction of the MTBR/proline-rich region (Figures 2H and 4A) and (b) no observable change in the most N-terminal segment of the projection domain (residues 17–103, Figure 2C).

Our FRET measurements find that heparin binding results in conformational changes in the MTBR and its flanking regions, including the latter half of the projection domain (residues 103–184, Figures 2D and 4B). This data is consistent with

previous work that mapped heparin binding to a lysine-rich region in the projection domain (residues 149–154) in addition to the MTBR and flanking proline-rich and C-terminal regions.<sup>46</sup> Interactions with heparin are generally electrostatic in nature,<sup>49</sup> and we find that NaCl is able to block the effects of heparin on the MTBR in a concentration-dependent manner (SI, Figure S3). High salt has been shown to inhibit heparin-induced aggregation<sup>33</sup> and to disrupt heparin-induced structure,<sup>42</sup> and our data suggest that such observations may derive mechanistically from altered interactions between heparin and the MTBR.

Strikingly, the most N-terminal portion of the projection domain (residues 17–103; Figure 2C) remains unchanged despite reconfiguration of other segments within the domain as well as overall reorientation of the domain with respect to the rest of the protein. This region of the projection domain is highly flexible<sup>40</sup> and is thought to be mostly disordered even in the MT-bound state<sup>50</sup> and in PHFs.<sup>51</sup> Intrinsic disorder is thought to confer functional diversity through binding promiscuity,<sup>52</sup> and tau interacts with numerous other cellular binding partners via its N-terminus.<sup>13</sup> Our measurements indicate that a highly extended conformational ensemble persists upon heparin binding, suggesting that maintaining these interactions may be possible even in the early stages of aggregation.

## DISCUSSION

Here we used single-molecule FRET to investigate the conformational ensemble of monomer tau. By independently probing multiple segments within the linear sequence of tau, we are able to observe domain-specific behavior of the protein. We find that the segments respond differentially to both heparin (Figure 2A–H) and salt (Figure 3A–D). Because intrinsically disordered proteins are enriched in polar and charged amino acids relative to globular proteins,<sup>53,54</sup> the electrostatic effect of salt on such proteins is worth further consideration. One recent study found that high salt caused collapse of a small intrinsically disordered protein, whereas it resulted in the expansion of a similarly sized denatured globular protein.<sup>38</sup> Polyampholyte theory was used to explain this behavior as a general property of these different classes of disordered proteins. Our results, which show that intrinsically disordered tau expands at high salt concentrations, seem at first glance to be in conflict with theory. However, considering the individual constructs is significantly more revealing. We constructed a charge–hydrophobicity plot<sup>54</sup> for all of the tau constructs used in this study (Figure 3E). Most fall relatively close to the intersection between disordered and globular proteins and the response of each construct to high salt is correlated with its position on this plot. To illustrate, the N-terminal projection domain, which collapses at high salt, displays the most intrinsically disordered protein-like characteristics of all our constructs probed (Figure 3C,E), while the C-terminal region, which is more similar to a globular protein with regard to charge and hydrophobicity, expands in high salt (Figure 3B,E). It has been previously noted through analysis by multiple disorder prediction software programs<sup>48</sup> and by NMR<sup>40</sup> that portions of the MTBR and the C-terminus may be partially folded despite the overall disordered characteristic of the full protein. Thus, on the level of the individual domains, our results are consistent with these studies and they illustrate that these domains may respond independently to changes in their local environment. Moreover, they emphasize that understanding both the

functional behavior and the aggregation of a large, multidomain intrinsically disordered protein like tau requires that the properties of the individual domains be considered.

On the basis of the differences in FRET in the absence and presence of heparin (Figure 2), we developed a coarse-grain model of the conformational changes relevant to the initiation of aggregation (Figure 5). In solution, our results describe a

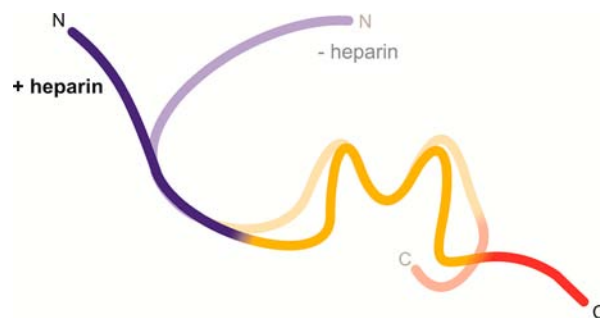


**Figure 5.** Model of conformational changes associated with population of an aggregation-prone conformational ensemble. Color coding of the regions corresponds to Figure 3: projection domain (blue), MTBR (yellow), and C-terminus (red) for tau in the absence (faded) and presence (bold) of heparin.

model of tau that retains long-range contacts between termini and between each terminus and the MTBR, leading to a relatively compact structure as compared to a RC. These results are qualitatively compatible with the compaction described previously by NMR<sup>40</sup> and by the proposed “paper-clip” structure for tau derived from ensemble FRET studies.<sup>55</sup> However, in contrast to the ensemble study, our single-molecule FRET results indicate that the distance between either terminus and the MTBR is smaller than the distance between the termini, such that our model when projected in two dimensions is more S-shaped than paper-clip-shaped. Additionally the distances calculated from our measured peak  $ET_{\text{eff}}$  values (SI, Table S3) are overall significantly ( $\sim 2$ – $4$  times) greater than comparable distances reported from the ensemble study.<sup>55</sup> This may be due to our use of probes that are capable of measuring larger distances ( $R_0$  of single-molecule FRET fluorophores Alexa 488 and Alexa 594 is 54 Å;  $R_0$  of ensemble FRET fluorophores tryptophan and IAEDANS is 22 Å) as well our use of a polymer model (SI) that reflects the conformation of ensembles sampled by a disordered protein more accurately than the standard Förster equation to convert from measured  $ET_{\text{eff}}$  to distance.<sup>56</sup>

In our model, heparin binding leads to a loss of long-range contacts between the termini (Figure 2A) and between each terminus and the MTBR (Figure 2B,G), accompanied by compaction of the MTBR and proline-rich region (Figures 2H and 4). The monoclonal antibodies Alz50 and MC1, which detect tau fibrillar pathology associated with AD, have been shown to interact with discontinuous epitopes on tau consisting of N-terminal and MTBR segments<sup>57,58</sup> potentially brought about by intra- or intermolecular interactions. Our results that show a loss of the N-terminal and MTBR contacts upon binding heparin would therefore support an intermolecular basis for these antibody interactions. The changes we observe may also represent a conformation of the tau monomer that precedes recognition by these antibodies, which have been shown to preferentially bind PHFs over monomeric tau.<sup>57</sup>

While it is striking that binding of heparin results in conformational changes throughout the tau sequence, the changes to the MTBR provide the most insight into aggregate formation, as it forms the core of PHFs.<sup>14</sup> The compaction observed upon heparin binding (Figures 2H and 4) is also found in truncated versions of the protein, even in the absence of heparin (SI, Figure S1). While we cannot infer secondary structure from our measurements, this compaction may represent an enhanced propensity for secondary structure, as previous NMR studies have indicated a propensity for elements of both  $\alpha$ -helix<sup>46,59</sup> and  $\beta$ -sheet<sup>40,46</sup> in this region. As both heparin binding and truncation are conditions that accelerate aggregation and cause compaction of the MTBR, we propose that the compact ensembles sampled under these conditions represent “aggregation-prone” conformations of tau and further suggest that the termini may prevent or restrict the sampling of conformations that are favorable for aggregation. Similar to what has been suggested for  $\alpha$ -synuclein in Parkinson’s disease,<sup>60</sup> loss of the native long-range contacts in tau may lead to enhancement of this state and consequent accelerated aggregation of tau.

## CONCLUSIONS

In this work we have characterized the ensemble of conformations sampled by tau in solution and have identified conformational changes associated with the initiation of aggregation. In our model, heparin binding to tau results in the loss of long-range interactions while concurrently promoting population of a more compact MTBR ensemble. This conformational state of tau represents a potential target for AD diagnostics and therapeutics aimed at altering the self-association of tau. Stabilization of native long-range interactions may prove to be a successful strategy for preventing tau aggregation in Alzheimer’s disease and tauopathies in general.

## ASSOCIATED CONTENT

### Supporting Information

Supporting description of the methods; quantification of heparin binding; aggregation, fluorescence anisotropy, and fluorescence lifetime controls; and calculation of distances from  $ET_{\text{eff}}$  values. This material is available free of charge via the Internet at <http://pubs.acs.org>

## AUTHOR INFORMATION

### Corresponding Author

elizabeth.rhoades@yale.edu

### Author Contributions

<sup>†</sup>The manuscript was written through contributions of all authors. All authors have given approval to the final version of the manuscript.

### Notes

The authors declare no competing financial interest.

## ACKNOWLEDGMENTS

The authors thank A. Miranker for critical reading of the manuscript, G. Cobb for help with lifetime measurements and aggregation assays, A. Nath for assistance with the figures, and L. Binder and L. Regan for the tau and pET-HT plasmids, respectively, used to create the full-length tau construct. This work was supported by NSF 0919853 (to E.R.) and National Institutes of Health 5T32GM007223-35 (to S.E.).

## ABBREVIATIONS

MAP, microtubule associated protein; MT, microtubule; PHF, paired helical filament; NFT, neurofibrillary tangle; AD, Alzheimer’s disease; FRET, Förster resonance energy transfer; FCS, fluorescence correlation spectroscopy.

## REFERENCES

- (1) Lee, V. M.; Goedert, M.; Trojanowski, J. Q. *Annu. Rev. Neurosci.* **2001**, *24*, 1121.
- (2) Buee, L.; Bussiere, T.; Buee-Scherrer, V.; Delacourte, A.; Hof, P. R. *Brain Res. Rev.* **2000**, *33*, 95.
- (3) Garcia, M. L.; Cleveland, D. W. *Curr. Opin. Cell. Biol.* **2001**, *13*, 41.
- (4) Goedert, M.; Spillantini, M. G. *Science* **2006**, *314*, 777.
- (5) Ballatore, C.; Lee, V. M.; Trojanowski, J. Q. *Nat. Rev. Neurosci.* **2007**, *8*, 663.
- (6) Cleveland, D. W.; Hwo, S. Y.; Kirschner, M. W. *J. Mol. Biol.* **1977**, *116*, 227.
- (7) Schweers, O.; Schonbrunnhanebeck, E.; Marx, A.; Mandelkow, E. *J. Biol. Chem.* **1994**, *269*, 24290.
- (8) von Bergen, M.; Barghorn, S.; Biernat, J.; Mandelkow, E. M.; Mandelkow, E. *Biochim. Biophys. Acta* **2005**, *1739*, 158.
- (9) Chiti, F.; Dobson, C. M. *Annu. Rev. Biochem.* **2006**, *75*, 333.
- (10) Drechsel, D. N.; Hyman, A. A.; Cobb, M. H.; Kirschner, M. W. *Mol. Biol. Cell* **1992**, *3*, 1141.
- (11) Gustke, N.; Trinczek, B.; Biernat, J.; Mandelkow, E. M.; Mandelkow, E. *Biochemistry* **1994**, *33*, 9511.
- (12) Mukrasch, M. D.; von Bergen, M.; Biernat, J.; Fischer, D.; Griesinger, C.; Mandelkow, E.; Zweckstetter, M. *J. Biol. Chem.* **2007**, *282*, 12230.
- (13) Avila, J.; Lucas, J. J.; Perez, M.; Hernandez, F. *Physiol. Rev.* **2004**, *84*, 361.
- (14) Crowther, T.; Goedert, M.; Wischik, C. M. *Ann. Med.* **1989**, *21*, 127.
- (15) von Bergen, M.; Friedhoff, P.; Biernat, J.; Heberle, J.; Mandelkow, E. M.; Mandelkow, E. *Proc. Natl. Acad. Sci. U. S. A.* **2000**, *97*, 5129.
- (16) Chirita, C. N.; Necula, M.; Kuret, J. *J. Biol. Chem.* **2003**, *278*, 25644.
- (17) Kuret, J.; Congdon, E. E.; Li, G.; Yin, H.; Yu, X.; Zhong, Q. *Microsc. Res. Tech.* **2005**, *67*, 141.
- (18) Chirita, C. N.; Congdon, E. E.; Yin, H.; Kuret, J. *Biochemistry* **2005**, *44*, 5862.
- (19) Zhao, H. X.; Tuominen, E. K. J.; Kinnunen, P. K. J. *Biochemistry* **2004**, *43*, 10302.
- (20) Elbaum-Garfinkle, S.; Ramlall, T.; Rhoades, E. *Biophys. J.* **2010**, *98*, 2722.
- (21) Crowther, R. A.; Olesen, O. F.; Jakes, R.; Goedert, M. *FEBS Lett.* **1992**, *309*, 199.
- (22) Kuret, J.; Chirita, C. N.; Congdon, E. E.; Kannanayakal, T.; Li, G.; Necula, M.; Yin, H.; Zhong, Q. *Biochim. Biophys. Acta* **2005**, *1739*, 167.
- (23) Barghorn, S.; Zheng-Fischhofer, Q.; Ackmann, M.; Biernat, J.; von Bergen, M.; Mandelkow, E. M.; Mandelkow, E. *Biochemistry* **2000**, *39*, 11714.
- (24) Wilson, D. M.; Binder, L. I. *Am. J. Pathol.* **1997**, *150*, 2181.
- (25) Taniguchi, S.; Suzuki, N.; Masuda, M.; Hisanaga, S.; Iwatsubo, T.; Goedert, M.; Hasegawa, M. *J. Biol. Chem.* **2005**, *280*, 7614.
- (26) Crowe, A.; Ballatore, C.; Hyde, E.; Trojanowski, J. Q.; Lee, V. M. Y. *Biochem. Biophys. Res. Commun.* **2007**, *358*, 1.
- (27) Glabe, C. G. *Neurobiol. Aging* **2006**, *27*, 570.
- (28) Glabe, C. G. *J. Biol. Chem.* **2008**, *283*, 29639.
- (29) Haass, C.; Selkoe, D. J. *Nat. Rev. Mol. Cell. Biol.* **2007**, *8*, 101.
- (30) Kaye, R.; Head, E.; Thompson, J. L.; McIntire, T. M.; Milton, S. C.; Cotman, C. W.; Glabe, C. G. *Science* **2003**, *300*, 486.
- (31) Friedhoff, P.; Schneider, A.; Mandelkow, E. M.; Mandelkow, E. *Biochemistry* **1998**, *37*, 10223.
- (32) Barghorn, S.; Mandelkow, E. *Biochemistry* **2002**, *41*, 14885.

- (33) Jeganathan, S.; von Bergen, M.; Mandelkow, E. M.; Mandelkow, E. *Biochemistry* **2008**, *47*, 10526.
- (34) Trexler, A.; Rhoades, E. *Biochemistry* **2009**, *48*, 2304.
- (35) Sevcik, E.; Trexler, A. J.; Dunn, J. M.; Rhoades, E. *J. Am. Chem. Soc.* **2011**, *133*, 7152.
- (36) Nath, A.; Miranker, A. D.; Rhoades, E. *Angew. Chem., Int. Ed.* **2011**, *50*, 10859.
- (37) Mukhopadhyay, S.; Krishnan, R.; Lemke, E. A.; Lindquist, S.; Deniz, A. A. *Proc. Natl. Acad. Sci. U. S. A.* **2007**, *104*, 2649.
- (38) Muller-Spath, S.; Soranno, A.; Hirschfeld, V.; Hofmann, H.; Ruegger, S.; Reymond, L.; Nettels, D.; Schuler, B. *Proc. Natl. Acad. Sci. U. S. A.* **2010**, *107*, 14609.
- (39) Sherman, E.; Haran, G. *Proc. Natl. Acad. Sci. U. S. A.* **2006**, *103*, 11539.
- (40) Mukrasch, M. D.; Bibow, S.; Korukottu, J.; Jeganathan, S.; Biernat, J.; Griesinger, C.; Mandelkow, E.; Zweckstetter, M. *PLoS Biol.* **2009**, *7*, 399.
- (41) Harbison, N. W.; Bhattacharya, S.; Eliezer, D. *PLoS One* **2012**, *7*, e34679.
- (42) Wegmann, S.; Scholer, J.; Bippes, C. A.; Mandelkow, E.; Muller, D. J. *J. Biol. Chem.* **2011**, *286*, 20512.
- (43) Schuler, B.; Lipman, E. A.; Eaton, W. A. *Nature* **2002**, *419*, 743.
- (44) Merchant, K. A.; Best, R. B.; Louis, J. M.; Gopich, I. V.; Eaton, W. A. *Proc. Natl. Acad. Sci. U. S. A.* **2007**, *104*, 1528.
- (45) Trexler, A. J.; Rhoades, E. *Biophys. J.* **2010**, *99*, 3048.
- (46) Sibille, N.; Sillen, A.; Leroy, A.; Wieruszkeski, J. M.; Mulloy, B.; Landrieu, I.; Lippens, G. *Biochemistry* **2006**, *45*, 12560.
- (47) Zhu, H. L.; Fernandez, C.; Fan, J. B.; Shewmaker, F.; Chen, J.; Minton, A. P.; Liang, Y. *J. Biol. Chem.* **2010**, *285*, 3592.
- (48) von Bergen, M.; Barghorn, S.; Jeganathan, S.; Mandelkow, E. M.; Mandelkow, E. *Neurodegener. Dis.* **2006**, *3*, 197.
- (49) Capila, I.; Linhardt, R. J. *Angew. Chem., Int. Ed.* **2002**, *41*, 391.
- (50) Santarella, R. A.; Skiniotis, G.; Goldie, K. N.; Tittmann, P.; Gross, H.; Mandelkow, E. M.; Mandelkow, E.; Hoenger, A. *J. Mol. Biol.* **2004**, *339*, 539.
- (51) Bibow, S.; Mukrasch, M. D.; Chinnathambi, S.; Biernat, J.; Griesinger, C.; Mandelkow, E.; Zweckstetter, M. *Angew. Chem., Int. Ed.* **2011**, *50*, 11520.
- (52) Tompa, P. *FEBS Lett.* **2005**, *579*, 3346.
- (53) Radivojac, P.; Iakoucheva, L. M.; Oldfield, C. J.; Obradovic, Z.; Uversky, V. N.; Dunker, A. K. *Biophys. J.* **2007**, *92*, 1439.
- (54) Uversky, V. N.; Gillespie, J. R.; Fink, A. L. *Proteins* **2000**, *41*, 415.
- (55) Jeganathan, S.; von Bergen, M.; Brutlach, H.; Steinhoff, H. J.; Mandelkow, E. *Biochemistry* **2006**, *45*, 2283.
- (56) Thirumalai, D.; O'Brien, E. P.; Morrison, G.; Brooks, B. R. *J. Chem. Phys.* **2009**, *130*.
- (57) Carmel, G.; Mager, E. M.; Binder, L. I.; Kuret, J. *J. Biol. Chem.* **1996**, *271*, 32789.
- (58) Jicha, G. A.; Bowser, R.; Kazam, I. G.; Davies, P. *J. Neurosci. Res.* **1997**, *48*, 128.
- (59) Eliezer, D.; Barre, P.; Kobaslija, M.; Chan, D.; Li, X. H.; Heend, L. *Biochemistry* **2005**, *44*, 1026.
- (60) Bertoncini, C. W.; Jung, Y. S.; Fernandez, C. O.; Hoyer, W.; Griesinger, C.; Jovin, T. M.; Zweckstetter, M. *Proc. Natl. Acad. Sci. U. S. A.* **2005**, *102*, 1430.